

Interface Engineering for Atomic Layer Deposited Alumina Gate Dielectric on SiGe Substrates

Liangliang Zhang¹, Yuzheng Guo², Vinayak Vishwanath Hassan³, Kechao Tang⁴, Majeed A. Foad³, Joseph C. Woicik⁵, Piero Pianetta⁶, John Robertson² and Paul C. McIntyre^{4*}

¹Department of Electrical Engineering, Stanford University, USA

²Engineering Department, Cambridge University, Cambridge CB2 1PZ, United Kingdom.

³Applied Materials, Santa Clara, CA, USA

⁴Department of Materials Science and Engineering, Stanford University, USA

⁵Materials Science and Engineering Laboratory, National Institute of Standards and Technology, Gaithersburg, Maryland, USA.

⁶SLAC National Accelerator Center, Menlo Park, CA 94025, USA

*email: pcm1@stanford.edu

Abstract

Optimization of the interface between high-k dielectrics and SiGe substrates is a challenging topic due to the complexity arising from the co-existence of Si and Ge interfacial oxides. Defective high-k/SiGe interfaces limit future applications of SiGe as a channel material for electronic devices. In this paper, we identify the surface layer structure of as-received SiGe and Al₂O₃/SiGe structures based on soft and hard x-ray photoelectron spectroscopy (PES). As-received SiGe substrates have native SiO_x/GeO_x surface layers, where the GeO_x-rich layer is beneath a SiO_x-rich surface. Silicon oxide regrows on the SiGe surface during Al₂O₃ ALD, and both SiO_x and GeO_x regrow during forming gas anneals (FGA) in the presence of a Pt gate metal. The resulting mixed SiO_x-GeO_x interface layer causes large interface trap densities (D_{it}) due to distorted Ge-O bonds across the interface. In contrast, we observed that oxygen-scavenging Al top gates decompose the underlying SiO_x/GeO_x, in a selective fashion, leaving an ultrathin SiO_x interfacial layer that exhibits dramatically reduced D_{it} .

P-type MOSFETs fabricated on SiGe substrates with high-k gate dielectrics are promising candidates to enhance MOS device performance due to the higher hole mobility of SiGe compared to Si¹⁻³. It is critical to obtain a good interface between the high-k gate oxide and SiGe for acceptable transistor performance. Silicon layers have been used in previous work as a passivation of the gate dielectric/SiGe interface, building on the excellent properties achieved with SiO₂/Si interfaces⁴, but this approach generates a trade-off between the interface quality and the scalability of the gate dielectric stack because SiO₂ has a lower dielectric constant than high-k materials. There are also reports of depositing various high-k dielectrics directly onto SiGe substrates, including Al₂O₃, ZrO₂, HfO₂, Y₂O₃, etc⁵⁻¹⁰. However, the co-existence of Si and Ge oxides at the surface introduces complexities that often produce an interface with unacceptably high defect density for MOS devices. A lack of detailed understanding of the influence of processing conditions on interface chemistry in high-k/SiGe devices prohibits the precise control of the thickness, trap density and stoichiometry of the surface oxides. In this work, we first characterize the surface layer structure of native oxides on as-received SiGe substrate using photoemission spectroscopy (PES). These defective sub-oxides can be removed by wet chemical etching, leaving an oxide-free (by synchrotron PES) SiGe surface. However, re-growth of interfacial SiO_x and GeO_x during ALD high-k deposition and subsequent annealing is almost unavoidable, and reintroduces a defective oxide/semiconductor interface. We then investigate the oxygen scavenging effect of a reactive (Al) top metal layer to control the thickness and composition of the interface oxide, and achieve very low-D_{it} SiGe MOS capacitors (MOSCAPs). Partial density of states (PDOS) are calculated based on first-principles modeling of GeO_x and SiO_x terminated SiGe surface structures. It is found that interface defects exist at GeO_x-terminated SiGe surface due to the distorted Ge-O bonds, whereas SiO_x-terminated SiGe has low interface trap densities

across the band gap. The simulation results are in good agreement with experimental data.

Fully-strained pseudomorphic p-type SiGe layers are epitaxially grown on lightly doped Si (100) substrates. Al₂O₃ films are atomic layer deposited with trimethyl aluminium (TMA) and H₂O as precursors. Fifty cycles of H₂O vapor prepulsing (pulse duration is 2 seconds, at a pressure of 0.67 Torr) is performed at 250°C to form a functionalized hydroxyl surface for better nucleation of the initial ALD cycles¹¹. For our ALD chamber, a temperature gradient is maintained from the unheated TMA bubbler to the chamber inlet of 120°C, and the substrate temperature is approximately 250°C. The growth rate of Al₂O₃ is 0.75 Å/cycle on a Si (100) wafer with vendor supplied chemical oxide layer of ~ 1.3 nm ellipsometric thickness. The Al₂O₃ growth per cycle is also measured by ellipsometry, after calibration by cross sectional transmission electron microscopy (TEM).

The photoelectron spectroscopy (PES) characterization are performed at Stanford Synchrotron Radiation Lightsource (SSRL) for soft x-ray PES, and at National Synchrotron Light Source (NSLS) beamline x24A for hard x-ray PES (HAXPES). SSRL beamline 8-1 provides energy ranges from 15 eV to 185 eV, with energy resolution ($\Delta E/E$) around 1×10^{-3} , and a spot size (defined by the FWHM) of ~ 0.1 mm². The photoelectrons are collected by a hemispherical electron energy analyser installed in an ultra-high vacuum chamber. The mean free path of electrons within this energy range is ~ 5 Å, so that this technique is very surface-sensitive, and does not resolve composition information at depths much greater than 1 nm below the sample surface. The PES chamber is kept under ultra-high vacuum ($\sim 1 \times 10^{-10}$ Torr), with the capability for angle resolved PES measurements. SSRL beamline 8-2 has a similar configuration, providing an energy range 100eV ~ 1300eV, with an energy resolution ($\Delta E/E$) around 4×10^{-4} . NSLS beamline x24A is equipped with an ultra-high vacuum chamber, and uses

constant-offset double-flat-crystal Golovchenko-Cowan design monochromator to select proper wavelengths. A Si (111) crystal is available to adjust the energy. Hard x-rays with energies ranging from 1.8 keV to 6 keV is provided. Details of the NSLS beamline x24A can be found in a previous report¹². The peak intensities for soft x-ray measurements are normalized to the incident beam intensities for fair comparisons among the spectra from different samples, some of the measured curves are vertically shifted for better display in the figures presented herein. For angle-resolved PES (ARPES) of core level peaks, we do not consider the fact that different momentum electrons can escape at different angles from the surface of the material¹³, because the core level states are so localized that they do not have significant k dispersions. It is also difficult to measure k dispersions at energies greater than several 10s of eVs, because momenta within the Brillouin zone are averaged over these energies. The main effect on peak intensity versus take-off angle is the different distance the excited electrons travel before leaving the surface.

Figure 1 (a) and (b) show the Si 2p and Ge 3d core levels, respectively, including chemically-shifted peaks of the oxides, collected with a photon energy of 140eV at SSRL beamline 8-1. The observed SiO_x and GeO_x peaks are from the native oxides on the top surface of the as-received samples. The fact that both Si 2p and Ge 3d elemental peaks are clearly detected suggests the native oxides are ultra-thin at the surface. The SiGe substrate with a larger Ge composition has larger GeO_x:Ge peak intensity ratios, suggesting more GeO_x is formed on the sample surface. The thickness of the interfacial oxides can be calculated from the area ratio of the oxide to substrate peaks in XPS using the Beer-Lambert equation, where an exponential decrease of electron flux as a function of travel distance is assumed¹⁴. It is found that the SiGe substrates have ~ 0.7 nm thick SiO_x films, and the GeO_x films are either 0.23 nm (for Si_{0.65}Ge_{0.35}) or 0.37 nm (Si_{0.55}Ge_{0.45}) in thickness. To determine the layered structure of the native oxides, we did ARPES to measure the Si 2p and Ge 3d regions. By normalizing the intensities to

that of the SiO_x peak, it is observed that the GeO_x peak decreases more strongly at smaller take-off angles, as shown in Figure 1(c). Combined with the above results, we can reach some general conclusions about the initial substrate surface composition: Both SiO_x and GeO_x are present in the thin native oxide, and GeO_x is concentrated beneath a superficial SiO_x -rich layer. This composite oxide layer is thicker for higher Ge composition SiGe epilayers, while the GeO_x -rich layer is thinner than the SiO_x -rich layer.

In order to make SiGe-MOSCAPs, the native oxide composite layer is first removed by cyclically cleaning the substrates with 2% HF (a.q.) and deionized (DI) water (with resistivity of 18.2 $\text{M}\Omega\cdot\text{cm}$) at room temperature (25°C). Si 2p and Ge 3d peaks of a cleaned sample are measured by lab-source x-ray photoelectron spectroscopy (XPS), using Al $k\text{-}\alpha$ radiation as the photon source with an energy of 1486.7 eV, as shown in Figure 2. The native oxides are effectively removed by the cyclic HF/DI-water clean, and their re-growth is slow enough that there is no observable growth during transfer of samples into the XPS chamber, as no SiO_x or GeO_x peaks are detected. Cleaned SiGe substrates are also quickly transferred into the loading chamber of our ALD system, with an air exposure time less than 1 min, to minimize contamination from the air. Figure 3 shows the Si 2p peaks of two as-grown ALD- Al_2O_3 /SiGe samples with a nominal 2.2 nm Al_2O_3 deposited at two different substrate temperatures. The spectra were measured by soft x-ray PES with a photon energy of 650 eV at SSRL beamline 8-2. Interfacial silicon oxide is regrown during Al_2O_3 ALD, so that high binding energy oxide tails appear on the Si 2p features of both samples. From the relative intensities of the Si peaks of SiGe substrate, it is evident that Al_2O_3 has a somewhat lower growth per cycle at higher ALD temperature, and more SiO_x is regrown at the Al_2O_3 /SiGe interface.

We have previously reported Pt-gated ALD- $\text{Al}_2\text{O}_3/\text{Ge}$ MOSCAPs with low interface trap density across the Ge band gap^{11,15,16}, where Pt helps dissociate molecular hydrogen to atomic hydrogen during forming gas (5% $\text{H}_2/95\%$ N_2) anneal (FGA). This passivates interface traps by 1) direct bonding of hydrogen to Ge interface defects and 2) promoting formation of a GeO_2 interface layer by reacting with residual hydroxyls in the Al_2O_3 layer to accelerate oxidation of the Ge surface. In some of the present experiments, Pt is used as the gate metal for SiGe MOSCAPs. A Pt gate of 70 nm thickness and a Ti 15nm/Al 50 nm back contact were deposited by e-beam evaporation. Post-metal FGA was performed at 350°C for 30 min. Figure 4(a) shows the C-V characteristics of a Pt-gated SiGe MOSCAP with 4 nm ALD- Al_2O_3 measured under frequencies ranging from 1kHz to 1MHz. The C-V curves are all distorted, even at 1 MHz, with large features related to traps observed in weak inversion, indicating the existence of defects at the interface. The possible origins of these defects include soft x-ray damage during the e-beam evaporation of the Pt gate, or intrinsic trap states related to dangling bonds at the $\text{Al}_2\text{O}_3/\text{SiGe}$ interface. Figure 5(a) and (b) show the normalized multi-frequency (1 kHz - 300 kHz) C-V characteristics of two SiGe MOSCAPs with thermally evaporated Pd (Figure 5(a)) and e-beam evaporated Pd (Figure 5(b)) as the gate metals. Palladium is used here instead of Pt because the melting point of Pt is too high for thermal evaporation, and Pd is also an efficient metal for catalysing H_2 dissociation to atomic hydrogen¹⁷. The C-V curves in Figure 5(a) and (b) are quite similar, both having similar capacitance features in weak inversion. Because thermal evaporation of Pd causes negligible soft x-ray exposure, the similar C-V curves indicate that these non-idealities in the C-V curves arise from intrinsic oxide/SiGe interface traps.

In order to probe the origin of the large apparent interface trap densities of Pt/ $\text{Al}_2\text{O}_3/\text{SiGe}$ capacitors shown in Figure 4(b), we use hard x-ray synchrotron photoelectron spectroscopy (HAXPES) to measure the photoelectrons from the

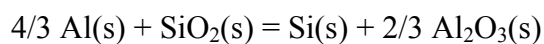
Al₂O₃/SiGe interface region and the SiGe substrate. Two samples with 5 nm e-beam evaporated Pt and 4 nm Al₂O₃ are used for HAXPES characterization, and one of them is annealed in forming gas for 30 minutes at 350°C. The fabrication process is identical to that of a MOSCAP, except that the Pt gate metal thickness is less. The photon energy used in this work is ~ 4029 eV, so that the excited electrons from core states have relatively long mean free path and electrons from the SiGe substrate can ballistically travel through the Al₂O₃ and Pt and emit from the top surface of the sample. The Si 1s and Ge 2p core levels of both samples are measured, as shown in Figure 6 (a) and (b). It has been reported previously that the binding energies of the chemically shifted oxide peaks of Si increase with increasing SiO₂ thickness. The relative shift difference $\Delta E(1s) - \Delta E(2p)$ is constant¹⁸, and several models have been proposed to explain the phenomenon, including local electronic relaxation, non-local image potential, etc. Reported SiO₂ peak (Si⁴⁺) shifts are > +4.3 eV for Si 1s for film thicknesses ranging from 0.4 nm to 4 nm¹⁸. The silicon oxide peaks detected in our work have a +3.7 eV shift from the Si 1s peak, suggesting that a sub-oxide, rather than SiO₂, is present at the interface. These SiO_x peaks are observed for both as-grown and post-FGA samples, where the intensity ratio of SiO_x to Si is larger for the latter samples. For the Ge 2p spectrum, no detectable GeO_x peak is observed for the as-grown sample, but there is a GeO_x tail for the sample after FGA. The above results indicate that both Si and Ge surfaces are oxidized to varying degrees during FGA.

Although it may appear to be unusual that both elements should be oxidized in a N₂/H₂ environment, this observation is consistent with the mechanism reported previously in reference 13. Atomic layer deposited Al₂O₃ films synthesized using the TMA/H₂O chemistry have been reported to contain residual hydroxyl species^{15,16,19,20}. Molecular hydrogen supplied by the forming gas, once dissociated to atomic hydrogen, can react with these hydroxyls (-OH) in Al₂O₃ to form H₂O, diffusion of which may transport oxygen to the Si or Ge surface to form interfacial SiO_x and GeO_x. The results

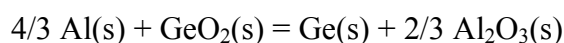
in Figure 6 indicate that formation of SiO_x is preferred in this process, as the GeO_x relative peak intensity is less than that of SiO_x .

Cross-sectional TEM is used to provide direct imaging of the multiple layers of films in a gate stack. As shown in Figure 7, the cross section TEM bright field image of a Pt/ Al_2O_3 /SiGe MOSCAP after FGA shows a thin region of reduced contrast only at the Al_2O_3 /SiGe interface that is consistent with an oxide interface layer between Al_2O_3 and the SiGe substrate, in keeping with the HAXPES results. As a result, using Pt and forming gas anneal forms a mixed SiO_x and GeO_x layer at the Al_2O_3 /SiGe interface. The presence of this mixed layer of silicon and germanium suboxides is correlated with the presence of electrically active defects at the interface.

Previous research on high-k/Si systems shows that a remote metal layer can extract oxygen from an ultrathin oxide layer at the high-k/Si interface, thus decomposing the oxide interlayer. With a thin titanium layer as an oxygen-scavenging overlayer, ZrO_2 /Si and HfO_2 /Si structures with thinned interface oxides were obtained, and the residual Si from the decomposed oxide regrows on the Si substrate epitaxially^{21,22}. In the original reports of interfacial SiO_2 decomposition using a remote Ti layer, no TiO_x phase formation was reported. Instead, the ability of titanium to dissolve oxygen at high concentrations as an interstitial solute was noted as a likely pathway for O scavenging²¹. Aluminium does not exhibit high solubility for oxygen²², but the reactions



and



have negative Gibbs free energy changes (e.g. $\Delta G^0 = -198.5\text{kJ}$ and -533.3kJ , respectively, at 298.15 K) based on standard Gibbs free energies of formation of the compounds²⁴, indicating that a thermodynamic driving force exists for oxygen scavenging from SiO_2 and GeO_2 by Al via formation of Al_2O_3 .

To investigate the different effects of Al and Pt gate metal processing on the underlying $\text{Al}_2\text{O}_3/\text{SiGe}$ interface, we designed an experiment illustrated schematically in Figure 8. An $\text{Al}_2\text{O}_3/\text{SiGe}$ sample was fabricated with the same ALD process used for MOSCAPs. The sample was then annealed in O_2 at 250°C for 15 min to form a $\text{SiO}_x/\text{GeO}_x$ oxide interlayer. SiO_x will appear at the interface before the O_2 anneal, but the detection of GeO_x is difficult because the amount of GeO_x is small, perhaps due to thermodynamic preference for silicon oxidation compared to germanium. We intentionally formed this oxide interface layer using an O_2 anneal, which increased the amount of $\text{SiO}_x/\text{GeO}_x$ to facilitate measurement of the oxide by PES through the thin metal coating. The sample was divided into two pieces, and thin (~ 2.5 nm) Al or Pt layers were evaporated on them. FGA at 350°C for 30 min was then performed on both samples. All samples were kept in a N_2 -purged dry box to minimize contamination and possible subcutaneous oxidation of the samples during storage prior to sample analysis.

We characterize both samples by soft x-ray PES at SSRL beamline 8-2 with photon energy 650 eV, and the results are shown in Figure 9. In this experiment, we are unable to analyse Al 2p spectra from the Pt/ $\text{Al}_2\text{O}_3/\text{SiGe}$ sample because of interference from the Pt $4f_{5/2}$ and $4f_{7/2}$ peaks which has binding energies 74.4 eV and 71.0 eV. The Pt peaks are so strong that Al 2p feature (binding energy 72.5 eV) cannot be characterized. We focus on Si 2p and Ge 3d core elemental features and their oxide peaks. Comparing the results from Al gated samples in Figure 9 (a) and (b) to those from Pt gated samples in Figure 9 (c) and (d), the intensity ratios of both GeO_x/Ge and SiO_x/Si are smaller for the Al gated sample, suggesting that it has less GeO_x and SiO_x at the $\text{Al}_2\text{O}_3/\text{SiGe}$

interface. Based on these results, Al gate metal appears to scavenge the oxygen from the underlying interface, leaving less SiO_x and, especially, less GeO_x at the interface.

In parallel with the PES studies, we fabricated Al-gated SiGe MOSCAPs using Al/ Al_2O_3 /SiGe gate stacks. Aluminium gates are made by e-beam evaporation and thermal evaporation, and their C-V characteristics are shown in Figure 10 (a) and (b). Both Al gate processes generate relatively ideal C-V curves, including small interface trap response and small frequency dispersion in depletion and weak inversion. Thermally evaporated Al following FGA at 400°C for 30 minutes generates the best C-V curves measured among all SiGe MOSCAPs we have studied. The D_{it} distribution across the bandgap of the thermal Al gated capacitor is extracted based on the full conductance model by step-by-step fitting the total capacitance and total conductance at multiple gate biases^{25,26}. The results are shown in Figure 10 (c), where any extracted D_{it} lower than $10^{10} \text{ eV}^{-1}\text{cm}^{-2}$ is set as $1 \times 10^{10} \text{ eV}^{-1}\text{cm}^{-2}$ because, for such tiny dispersion, it is hard to differentiate interface traps from random fluctuations in capacitance and conductance caused by measurement error. The D_{it} distribution exhibits a peak value ($\sim 7 \times 10^{11} \text{ eV}^{-1}\text{cm}^{-2}$) near the valence band, and a smaller peak ($\sim 2 \times 10^{11} \text{ eV}^{-1} \text{ cm}^{-2}$) near the middle of the bandgap. As a comparison study, the D_{it} values of Pt gated sample are shown in Figure 4(b), which are on the order of $10^{12} \text{ eV}^{-1}\text{cm}^{-2}$, and can exceed $10^{13} \text{ eV}^{-1}\text{cm}^{-2}$ at $\sim 0.3 \text{ eV}$ above the valence band edge. The D_{it} values of Al gated MOSCAPs are significantly lower than those of Pt gated samples. The electrical results indicate that oxygen scavenging by Al decomposes the GeO_x component of the interfacial oxide during annealing dramatically reduces D_{it} . A cross-section TEM bright field image of a post-FGA Al/ Al_2O_3 /SiGe MOSCAP is shown in Figure 11. In contrast to the Pt/ Al_2O_3 /SiGe MOSCAP in Figure 7, uniform contrast in the Al_2O_3 region and no detectable interface layer are observed, consistent with the PES-measured removal of the interface germanium oxide and thinning of silicon oxide.

Density functional theory based calculations with plane wave pseudopotential code CASTEP²⁷ are performed to further investigate the interfacial defects. A PBE-style generalized gradient approximation is used to calculate the exchange correlation energy²⁸. GeO_x-terminated and SiO_x-terminated SiGe:oxide interfaces are generated on the (100) surface of a SiGe crystal with Si:Ge ratio 3:2 (randomly mixed in the diamond structure), an approximation of the ratio 0.55:0.45 for SiGe used in most of the experiments. The GeO_x or SiO_x interfaces are capped with amorphous Al₂O₃ layers generated by ab initio molecular dynamics quenching from 3000K to 300K. The cell is also relaxed to minimize the force at the interface. The same parameters are used as in our previous works^{15,29}.

The total DOS for either a GeO_x or an SiO_x interface oxide are shown in Figure 12 (a) and (b), as well as the calculated electron spin orbitals of the defect states and the valance band maximum. The SiO_x-terminated SiGe surface has no gap states, while the GeO_x-terminated surface has several defect states across the whole band gap. The calculated DOS plots in Figure 12 are in excellent agreement with the D_{it} profiles extracted from experiment, as shown in Figure 4(b) and Figure 10(c). The Si:SiO_x interface and Ge:GeO_x interface differ in a number of ways. The defect states at the Si:SiO₂ interface induced by dangling bonds or anti-bonding have an extremely low density. Besides, those defect states are not deep in the SiGe gap, usually near the band edges^{30,31}. In contrast, the Ge:GeO_x interface is notorious for its high defect density and multiple defect states in the band gap¹⁵. Compared to Si-O bonds, Ge-O bonds are much weaker, and even twisted bond angles can cause some defect states in the gap. Two illustrations of near-interface bonding in Fig. 12 show defect orbitals for both interfaces. Figure 12(a) exhibits the defect orbitals in a Ge-terminated interface in the band gap

(with the PDOS shown in Figure 12 (b)). The defects are mainly localized at the Ge and O atoms at the interface. Gap states in the case of a Ge-terminated interface arise from the interfacial Ge atoms with the slightly distorted Ge-O bonds. The band edge of SiGe is in between that of pure Si and pure Ge³². Therefore, shallow defect states present at the Si:SiO₂ interface partially spread beyond the band edges, and will not act as interface traps. In contrast, the Ge:GeO_x interface defects remain in the band gap, as illustrated in Figure 1(a) of reference 32. It is well known that the generalized gradient approximation (GGA) will underestimate the band gap of SiGe^{33,34}, thus our calculated band gap of SiGe is around 0.2 eV smaller than the expected value for a Si:Ge ratio of 0.55:0.45³⁵. These theoretical calculations support the conclusion derived from experiment that removing the interfacial GeO_x can dramatically improve interface quality for SiGe MOS.

In summary, characterization of as-received SiGe substrates (with 35% and 45% Ge compositions) indicates the presence of a bilayer SiO_x/GeO_x surface oxide detected by photoemission. This native surface oxide is composed of a ~0.7 nm SiO_x-rich layer on the top surface, and a 0.2 ~ 0.3 nm thickness GeO_x-rich layer between SiO_x and the SiGe substrate. Re-growth of SiO_x/GeO_x after HF etching of the SiGe substrate surface during Al₂O₃ ALD and post-metal FGA is observed. Platinum-gated SiGe MOSCAPs have large interface trap densities due to intrinsic defects that result from the chemical bonding of the regrown SiO_x/GeO_x layer to the SiGe channel surface. In contrast, remote oxygen scavenging by an Al gate metal layer can decompose the complex SiO_x-GeO_x interface oxide layer during FGA, producing a much lower D_{it} interface and leaving a thin residual ultrathin SiO_x interlayer in the high-k/SiGe gate stack. First principle calculations of PDOS on GeO_x/SiGe and SiO_x/SiGe structures reveal that the defect states within the band gap in Ge-terminated interface are localized to the Ge or O

atoms and can be attributed to the slightly distorted Ge-O bonds of interfacial Ge atoms, while the Si-terminated interface is defect-free across the band gap.

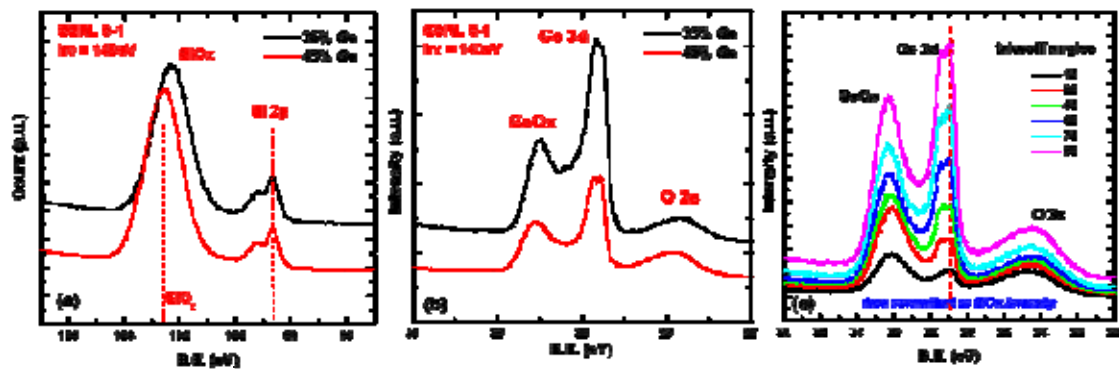


Figure 1: soft x-ray photoelectron spectroscopy (PES) of as-received SiGe substrates with native oxides, with binding energies in (a) Si 2p and SiO_x and (b) Ge 3d, GeO_x and O 2s regions. (c) Ge 3d, GeO_x and O 2s peaks of as-received SiGe measured by ARPES.

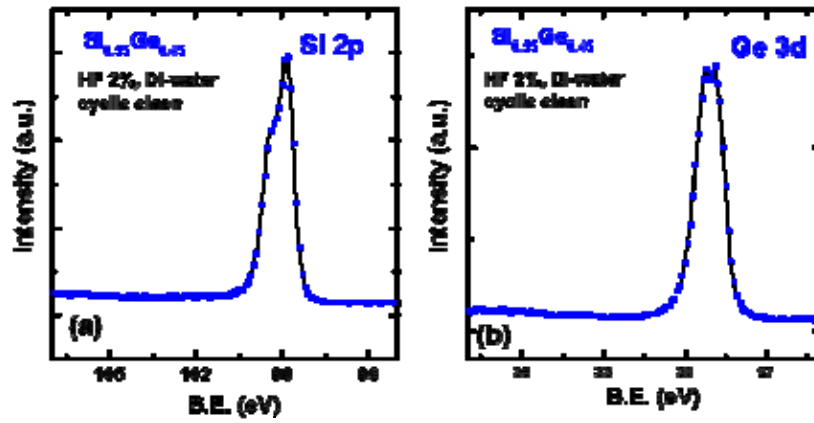


Figure 2 (a) (b) HF and DI-water cyclic cleaned $\text{Si}_{0.55}\text{Ge}_{0.45}$ substrates.

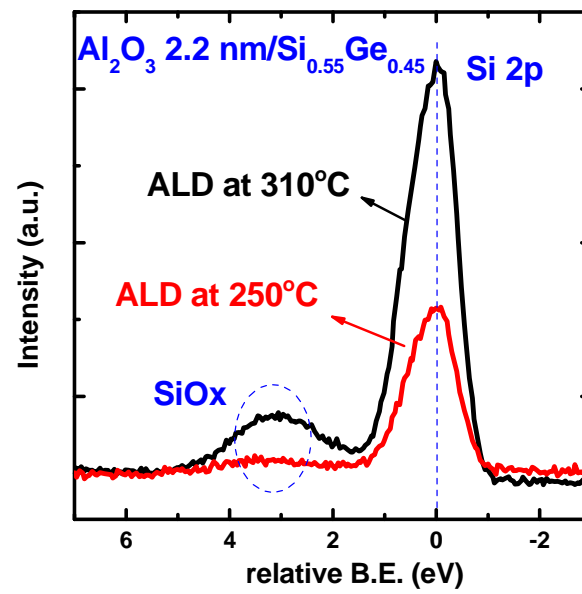


Figure 3 Soft x-ray PES of Si 2p region of as-grown Al₂O₃ 2.2 nm on Si_{0.55}Ge_{0.45} samples with ALD temperature at 250°C and 310°C.

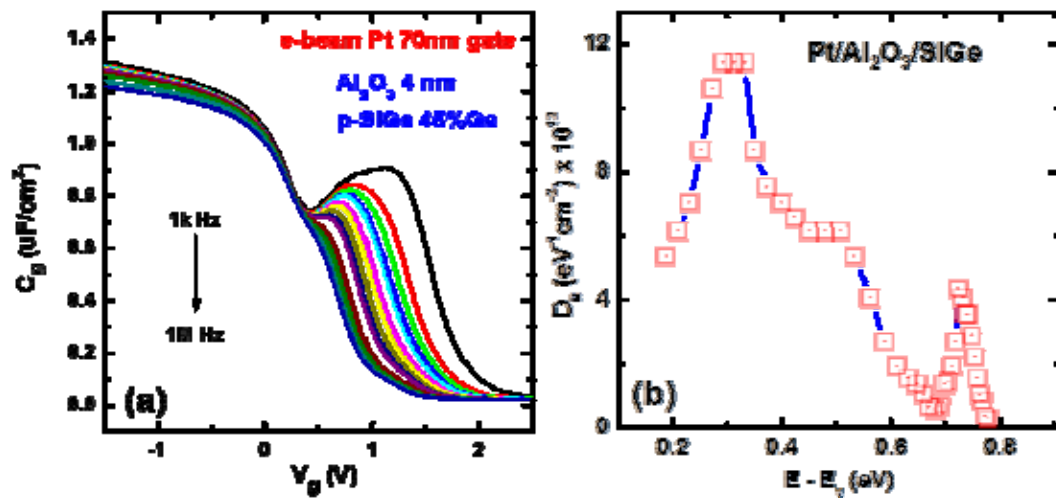


Figure 4 (a) C-V characteristics of a Pt/Al₂O₃/p- Si_{0.55}Ge_{0.45} MOSCAP. (b) the D_{it} distribution of the Pt/Al₂O₃/p- Si_{0.55}Ge_{0.45} MOSCAP within the bandgap extracted by full conductance model.

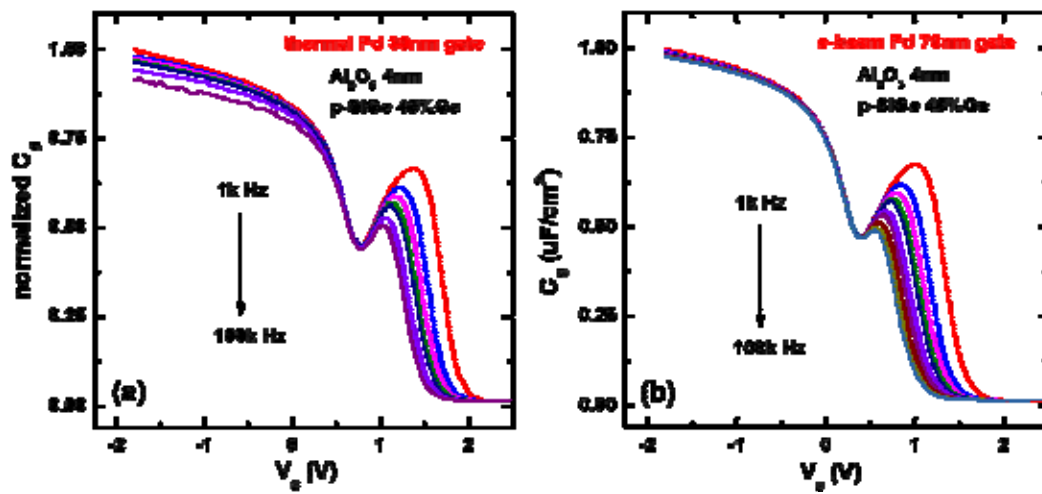


Figure 5 (a) normalized C-V characteristics of thermal evaporated Pd/ Al_2O_3 / $p\text{-Si}_{0.55}\text{Ge}_{0.45}$ MOSCAP. (b) normalized C-V characteristics of e-beam evaporated Pd/ Al_2O_3 / $p\text{-Si}_{0.55}\text{Ge}_{0.45}$ MOSCAP.

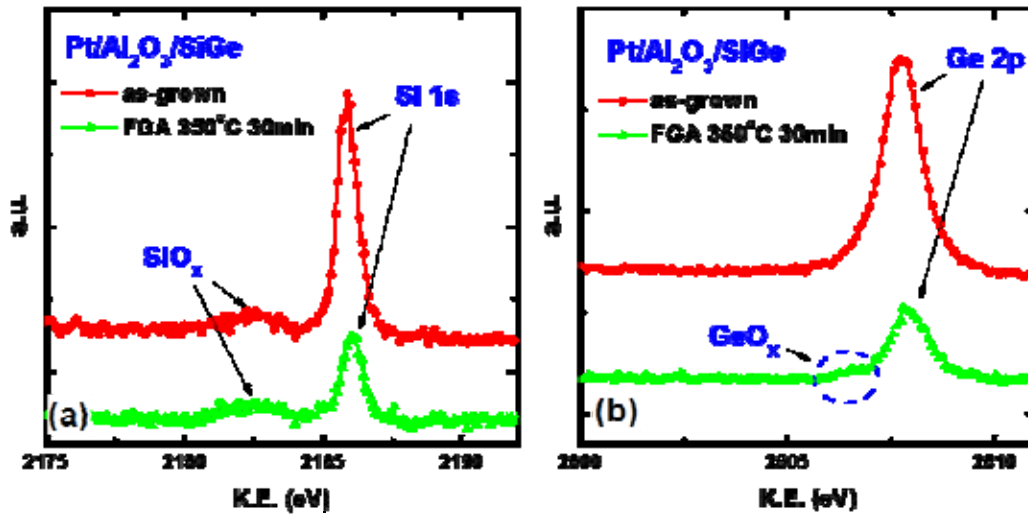


Figure 6 HAXPES measurement on Pt/Al₂O₃/Si_{0.55}Ge_{0.45} samples before (as-grown) and after FGA. (a) Si 1s region, (b) Ge 2p region.

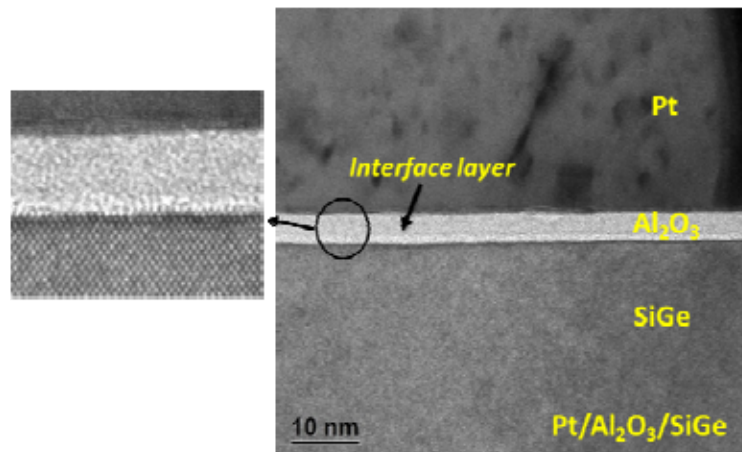


Figure 7 Cross section TEM of a Pt/Al₂O₃/ Si_{0.55}Ge_{0.45} MOSCAP after FGA at 350°C for 30 minutes.

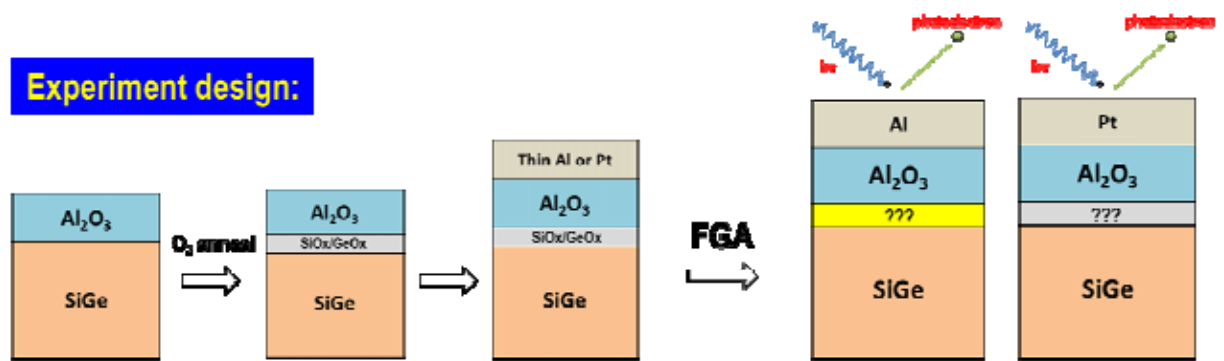


Figure 8 Illustration of the experiment design to investigate the different effect of Al and Pt on the $\text{Al}_2\text{O}_3/\text{SiGe}$ interface.

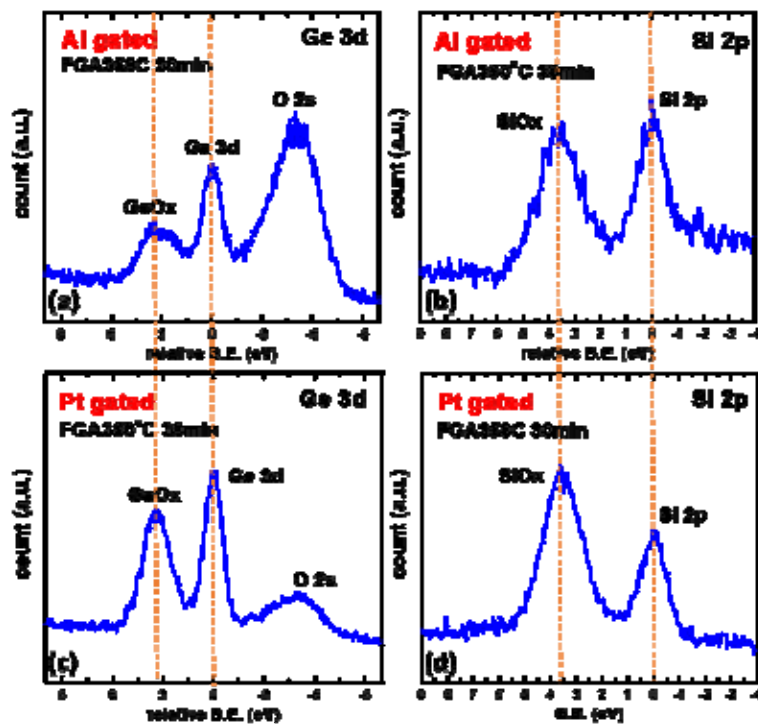


Figure 9. Soft x-ray PES characterization on Al or Pt gated $\text{Al}_2\text{O}_3/\text{SiGe}$ samples. (a) Al/ Al_2O_3 /SiGe, Ge 3d and O 2s spectra. (b) Al/ Al_2O_3 /SiGe, Si 2p spectrum. (c) Pt/ Al_2O_3 /SiGe, Ge 3d and O 2s spectra. (d) Pt/ Al_2O_3 /SiGe, Si 2p spectrum.

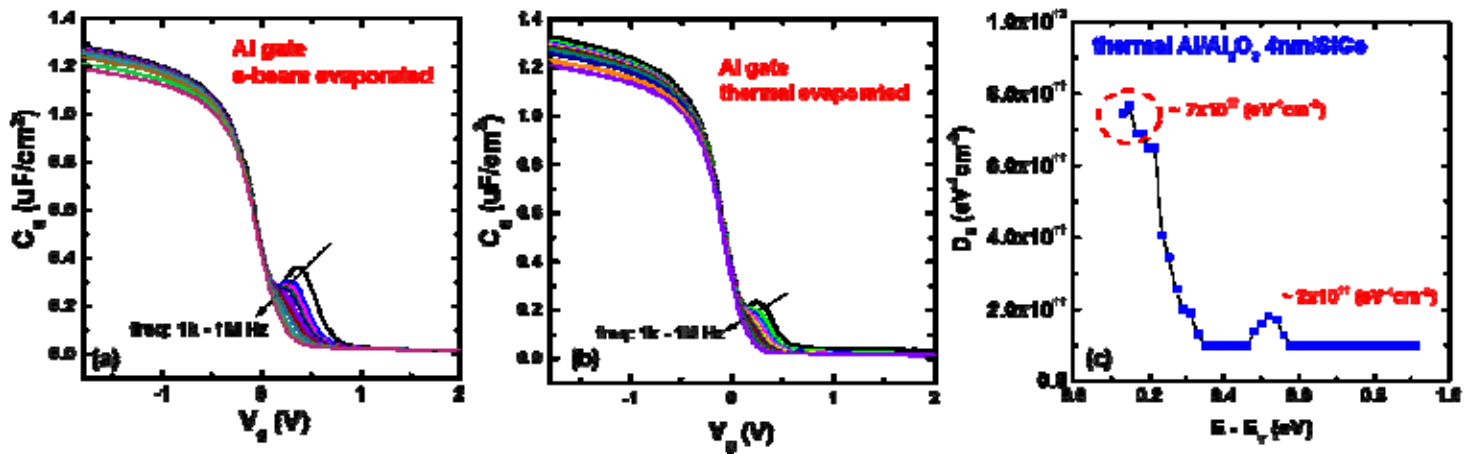


Figure 10. Al/ Al_2O_3 /SiGe MOSCAPs with (a) e-beam evaporated Al or (b) thermal evaporated Al gate. The thickness of Al gates is 100nm and the Al_2O_3 film thickness = 4 nm. Both samples are annealed with FGA at 400°C for 30 minutes.

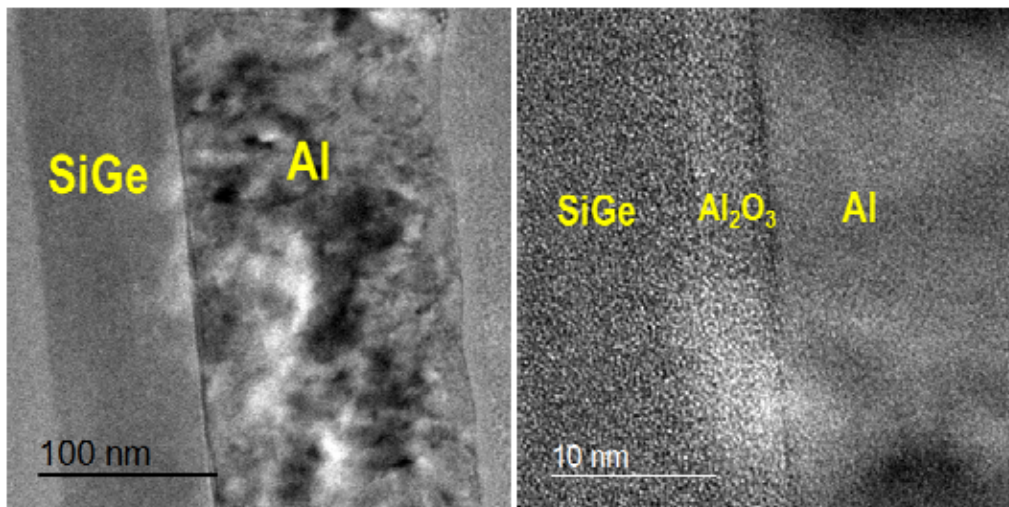


Figure 11. cross section TEM of Al/Al₂O₃/SiGe MOSCAPs after FGA 400°C for 30min with (left) lower magnification and (right) higher magnification.

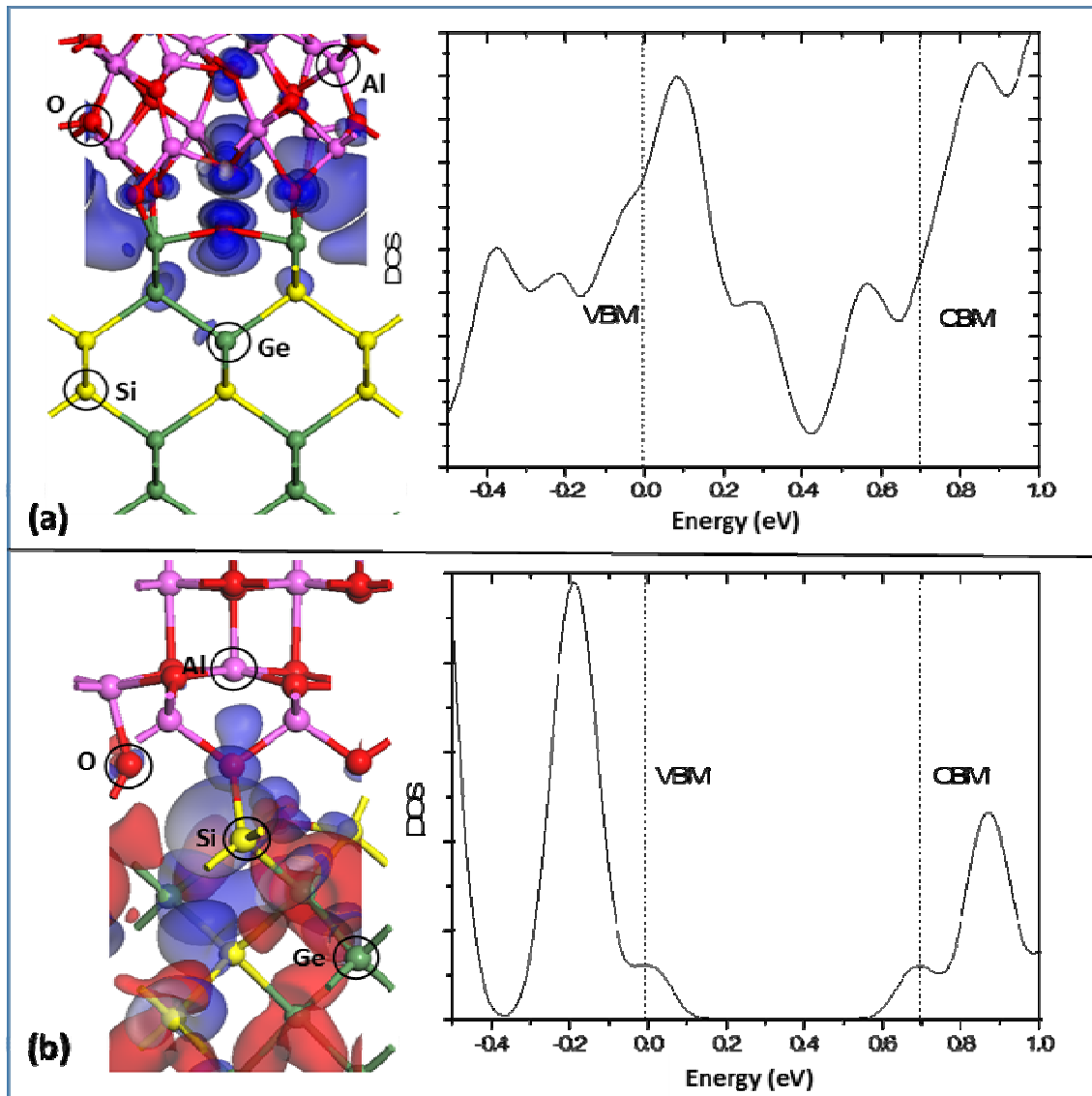


Figure 12. DFT simulation of $\text{Al}_2\text{O}_3/\text{SiGe}$ structures with (a) GeO_x interface and (b) SiO_x interface. Al - pink, O - red, Ge - green, yellow - Si. The density of states (DOS) is calculated with a smearing width of 0.1eV. In Figure (a), the blue orbitals at the interfaces are the defect states in the band gap as shown in the DOS. In Figure (b), the blue orbitals are the states at the valence and conduction band edges since there is no defect states in the band gap. The VBM and CBM are shown in red and blue respectively, both of which are localized across the SiGe part.

References

1. K. J. Kuhn, A. Murthy, R. Kotlyar, and M. Kuhn, Past, Present and Future: SiGe and CMOS Transistor Scaling, in *ECS Transactions*, **33** (6) 3-17 (2010).
2. P. Nguyen, S. Barraud, C. Tabone, L. Gaben, M. Cassé, F. Glowvacki, J.-M. Hartmann, M.-P. Samson, V. Maffini-Alvarro, C. Vizioz, N. Bernier, C. Guedj, C. Mounet, O. Rozeau, A. Toffoli, F. Allain, D. Delprat, B.-Y. Nguyen, C. Mazuré, O. Faynot and M. Vinet*, Dual-channel CMOS co-integration with Si NFET and strained-SiGe PFET in nanowire device architecture featuring sub-15nm gate length, in *IEEE International Electron Devices Meeting (IEDM)*, 2014.
3. P. Hashemi, K. Balakrishnan, S. Engelmann, J.A. Ott, A. Khakifirooz, A. Baraskar, M. Hopstaken, J.S. Newbury, K. Chan, E. Leobandung, R. Mo and D.G. Park, First Demonstration of High-Ge-Content Strained-Si_{1-x}Ge_x (x=0.5) on Insulator PMOS FinFETs with High Hole Mobility and Aggressively Scaled Fin Dimensions and Gate Lengths for High-Performance Applications, in *IEEE International Electron Devices Meeting (IEDM)*, 2014.
4. Noriyuki Taoka, Masatomi Harada, Yoshimi Yamashita, Toyoji Yamamoto, Naoharu Sugiyama and Shin-ichi Takagi, Effects of Si passivation on Ge metal-insulator-semiconductor interface properties and inversion-layer hole mobility, in *Appl. Phys. Lett.* **92**, 113511 (2008).
5. D. Wu, J. Lu, E. Vainonen-Ahlgren, E. Tois, M. Tuominen, M. Östling, S.-L. Zhang, Structural and electrical characterization of Al₂O₃/HfO₂/Al₂O₃ on strained SiGe, in *Solid-State Electronics*, Vol. 49, Issue 2, Feb. 2005, pp.193–197.
6. J.-H. Han, R. Zhang, T. Osada, M. Hata, M. Takenaka, S. Takagi, Impact of plasma post-nitridation on HfO₂/Al₂O₃/SiGe gate stacks toward EOT scaling, in *Microelectronic Engineering*, Vol 109, Sep. 2013, pp.266–269.

7. Reduction in Interface Trap Density of Al₂O₃/SiGe Gate Stack by Electron Cyclotron Resonance Plasma Post-nitridation, in *Applied Physics Express*, 6(5), Apr. 2013.
8. T. Ngai, W. J. Qi, R. Sharma, J. Fretwell, X. Chen, J. C. Lee and S. Banerjee, Electrical properties of ZrO₂ gate dielectric on SiGe, in *Appl. Phys. Lett.*, 76, 502 (2000).
9. Tobin Kaufman-Osborn, Evgueni A. Chagarov, Sang Wook Park, Bhagawan Sahu, Shariq Siddiqui, Andrew C. Kummel, atomic imaging and modeling of passivation, functionalization, and atomic layer deposition nucleation of the SiGe (001) surface via H₂O₂(g) and trimethylaluminum dosing, in *Surface Science*, Vol 630, Dec. 2014, pp.273–279
10. Evgueni Chagarov, Kasra Sardashti, Tobin Kaufman-Osborn, Shailesh Madiseti, Serge Oktyabrsky, Bhagawan Sahu, and Andrew Kummel, Density-Functional Theory Molecular Dynamics Simulations and Experimental Characterization of Al₂O₃/SiGe Interfaces, in *ACS Appl. Mater. Interfaces*, 7 (47), pp 26275–26283, Nov. 2015.
11. Swaminathan, S.; Oshima, Y.; Kelly, M. A.; McIntyre, P. C. Oxidant Prepulsing of Ge (100) Prior to Atomic Layer Deposition of Al₂O₃: In Situ Surface Characterization. *Appl. Phys. Lett.*, 2009, 95, 032907.
12. Weiland, C.; Rumaiz, A.; Lysaght, P.; Karlin, B.; Woicik, J.; Fischer, D. NIST, High Throughput Variable Kinetic Energy Hard X-Ray Photoelectron Spectroscopy Facility, *J. Electron Spectrosc. Relat. Phenom.*, 190, pp.193-200, 2013, DOI: 10.1016/j.elspec.2013.04.008.

13. Andrea Damascelli, Zahid Hussain, and Zhi-Xun Shen, Angle-resolved photoemission studies of the cuprate superconductors, *Rev. Mod. Phys.* **75**, 473, 2003.
14. M. F. Hochella Jr. and A. H. Carim, A reassessment of electron escape depths in silicon and thermally grown silicon dioxide thin films, in *Surface Science*, Vol. 197, Issue 3, pp.L260-L268, 1988.
15. Liangliang Zhang, Huanglong Li, Yuzheng Guo, Kechao Tang, Joseph Woicik, John Robertson and Paul C McIntyre, Selective Passivation of GeO₂/Ge Interface Defects in Atomic Layer Deposited High-k MOS Structures, in *ACS Applied Materials & Interfaces* **7** (37), 20499-20506, 2015.
16. Liangliang Zhang, Marika Gunji, Shruti Thombare, Paul C McIntyre, EOT Scaling of on Germanium pMOSFETs and Impact of Gate Metal Selection, in *IEEE Electron Device Letters*, **34** (6), 732-734, 2012.
17. T. Mitsui¹, M. K. Rose^{1,2}, E. Fomin^{1,2}, D. F. Ogletree¹ & M. Salmeron, Dissociative hydrogen adsorption on palladium requires aggregates of three or more vacancies, in *Nature* **422**, 705-707, Apr. 2003.
18. Th. Eickhoff, V. Medicherla, W. Drube, Final state contribution to the Si 2p binding energy shift in SiO₂/Si (100), in *J. El. Spec. and Rel. Phenom.*, vol. 137-140, pp. 85-88, July 2004.
19. Swaminathan, S.; Sun, Y.; Pianetta, P.; McIntyre, P. C. Ultrathin ALD-Al₂O₃ Layers for Ge (001) Gate Stacks: Local Composition Evolution and Dielectric Properties. *J. Appl. Phys.*, **110**, 094105-1-6, 2010.
20. M. D. Groner, F. H. Fabreguette, J. W. Elam and S. M. George, Low-Temperature Al₂O₃ Atomic Layer Deposition, in *Chem. Mater.*, **16**, 639-645, 2004.

21. Hyoungsub Kim, Paul C. McIntyre, Chi On Chui, Krishna C. Saraswat and Susanne Stemmer, Engineering chemically abrupt high-k metal oxide/silicon interfaces using an oxygen-gettering metal overlayer, in *J. Appl. Phys.*, 2004; 96 (6): 3467-3472.
22. Kang-Ill Seo, Dong-Ick Lee, Piero Pianetta, Hyoungsub Kim, Krishna C. Saraswat and Paul C. McIntyre, Chemical states and electrical properties of a high-k metal oxide/silicon interface with oxygen-gettering titanium-metal-overlayer, in *Appl. Phys. Lett.*, 2006; 89 (14).
23. H. A. Wriedt, The Al-O (Aluminum-Oxygen) System, in *Bull. Alloy Phase Diagrams*, **6**, 548– 553, 1985.
24. William M. Haynes, CRC Handbook of Chemistry and Physics, 95th ed., June 4, 2014 by CPC press, ISBN 9781482208689 - CAT# KE24083.
25. Yuan, Y.; Yu, B.; Ahn, J.; McIntyre, P. C.; Asbeck, P. M.; Rodwell, M. J. W.; Taur, Y. A Distributed Bulk-Oxide Trap Model for Al₂O₃ InGaAs MOS Devices. *IEEE Trans. Electron Devices*, 2012, 2100 - 2106.
26. Chen, H.-P.; Yuan, Y.; Yu, B.; Ahn, J.; McIntyre, P. C.; Asbeck, P. M.; Rodwell, M. J. W.; Taur, Y. Interface-State Modeling of Al₂O₃-InGaAs MOS From Depletion to Inversion. *IEEE Trans. Electron Devices*, 2012, 59, 9, 2383–2389.
27. Clark, S J; Segall, M D; Pickard, C J; Hasnip, P J; Probert, M J; Refson, K; Payne, M C. First principles methods using CASTEP., *Zeitschrift für Kristallographie*, Vol. 220, No. 5-6, 2005, p. 567-570.
28. Perdew, John P.; Burke Kieron; Ernzerhof Matthias; Generalized Gradient Approximation Made Simple, *Phys. Rev. Lett.* 77, 3865.
29. Y Guo, L Lin, J Robertson, Nitrogen Passivation at GaAs: Al₂O₃ Interfaces, *Applied Physics Letters* 102 (9), 091606.

30. Kwok-On Ng and David Vanderbilt, Structure and Oxidation Kinetics of the Si(100)-SiO₂ Interface, *Phys. Rev. B*, 59, 10132 (1999).
31. Yuhai Tu and J. Tersoff, Structure and Energetics of the Si- SiO₂ Interface, *Phys. Rev. Lett.* 84, 4393 (2000).
32. James T. Teherani, Winston Chern, Dimitri A. Antoniadis, Judy L. Hoyt, Liliana Ruiz, Christian D. Poweleit, and José Menéndez, Extraction of large valence-band energy offsets and comparison to theoretical values for strained-Si/strained-Ge type-II heterostructures on relaxed SiGe substrates, *Phys. Rev. B*, 85, 205308 (2012).
33. C. S. Wang and B. M. Klein, First-principles electronic structure of Si, Ge, GaP, GaAs, ZnS, and ZnSe. II. Optical properties, *Phys. Rev. B* 24, 3417, Sep. 1981.
34. Fabien Tran and Peter Blaha, Accurate Band Gaps of Semiconductors and Insulators with a Semilocal Exchange-Correlation Potential, *Phys. Rev. Lett.* 102, 226401, June 2009.
35. Srinivasan Krishnamurthy, A Sher, An - Ban Chen, Generalized Brooks' formula and the electron mobility in Si_xGe_{1-x} alloys, *Appl. Phys. Lett.* 47 ,1985, 160.